Supplementary Figures

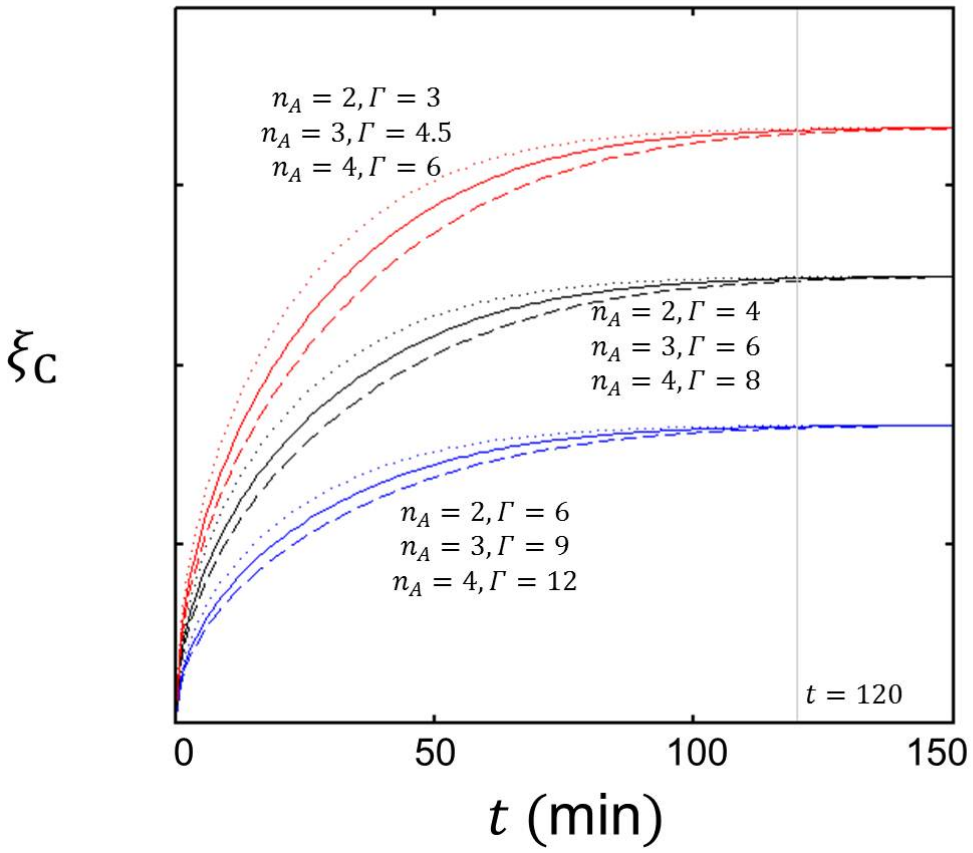

Supplementary Figure 1. Dynamic profiles of the critical position show the importance of a balance between scaling power and system attribute. Shown are numerical solutions of the critical position ξ_C for different parameter values of the scaling power n_A and the system attribute Γ with $n_D = n_w = 0$ and $\omega = 0.05$ min^{-1}. As the patterning system approaches steady state (with respect to morphogen gradient formation) when $t > 120$ min (gray bar), only the ratio n_A / Γ is relevant to ξ_C.

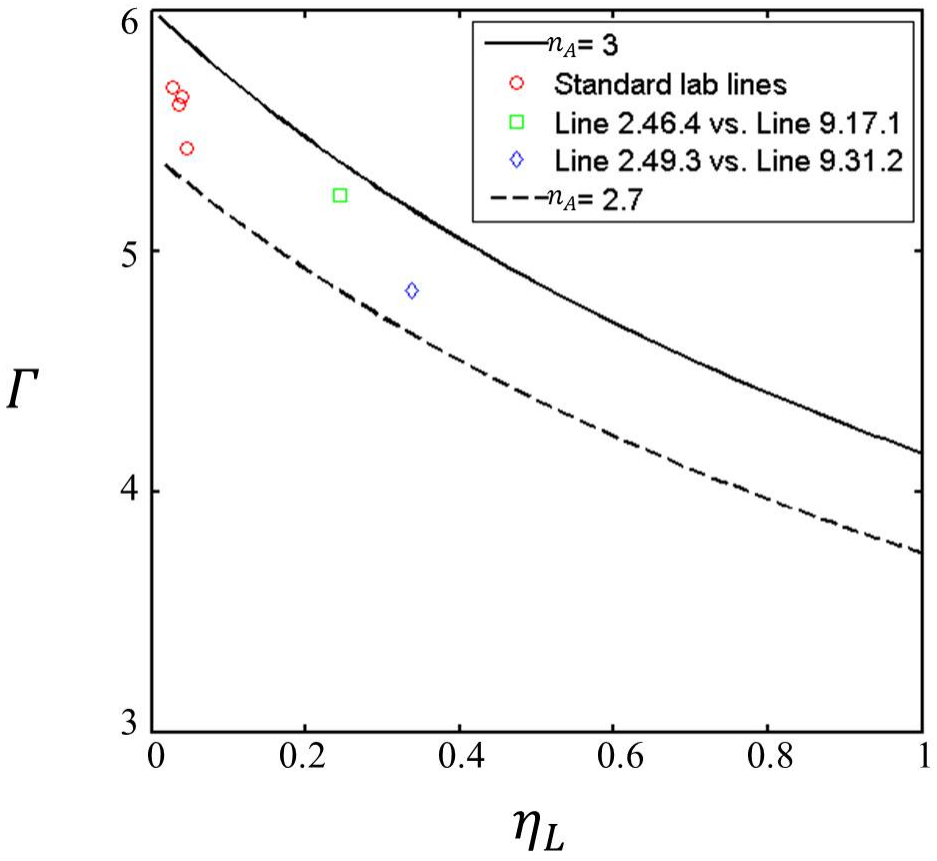

Supplementary Figure 2. Evaluating the relationship between *L* variation and scaling in discrete experimental populations. Shown are scatter plots of the system attribute Γ against the fractional variation in embryo length η_L measured from four standard lab lines with nominal *L* variations (red circles) or pairs of inbred lines with enhanced *L* variations and available side-by-side experimental data (green square and blue diamond). The solid and dashed lines represent the theoretical predictions for n_A = 3 and 2.7, respectively. Original sources of Bcd staining data used in this analysis are: standard lab lines w^{1118} (ref [1]), bcd^{E1}/+ (ref [1]), *stau* (ref [1]) and Cyo-*bcd*/+ (ref [2]); inbred lines #2.46.4 and #9.17.1 (ref [3]); inbred lines #2.49.3 and #9.31.2 (ref [4]).

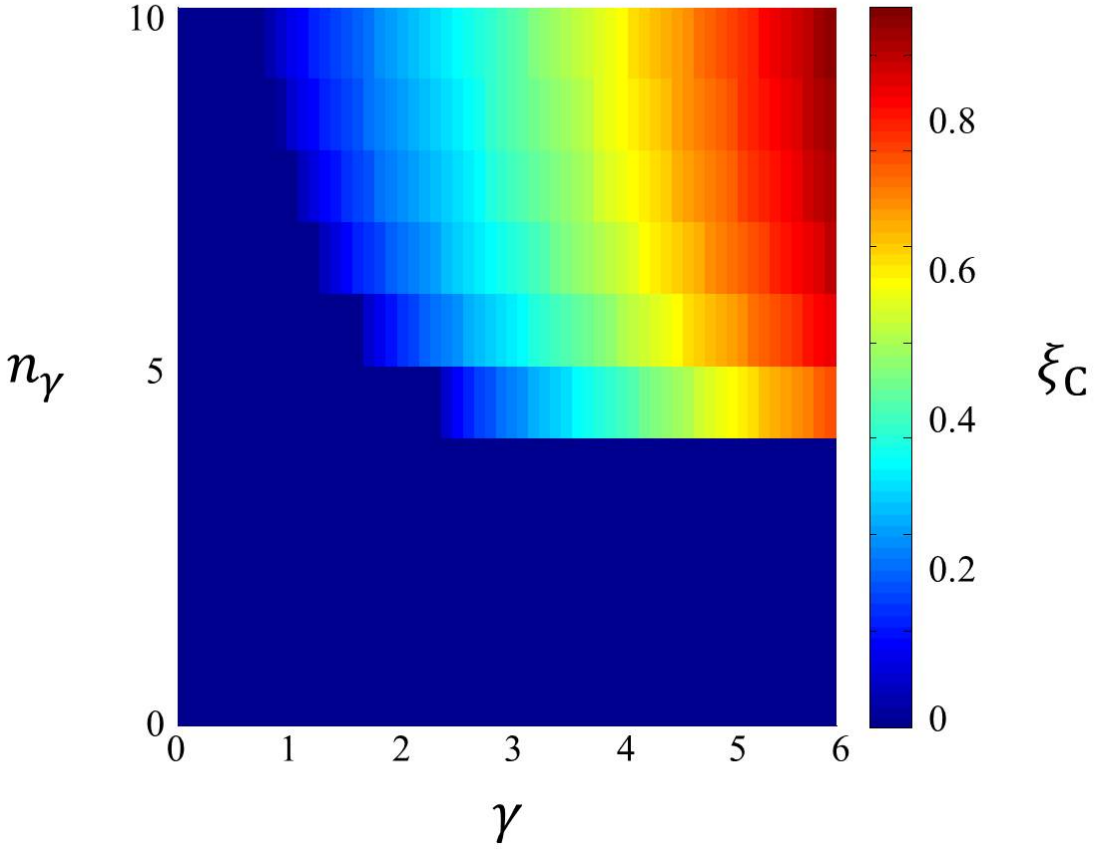

Supplementary Figure 3. No meaningful critical position within the source region is found unless the scaling power of source size is excessively large. The heat map shows the numerical solutions of the critical position ξ_C (in color) as a function of the relative size of the source region γ and the scaling power of source size n_γ. When $n_\gamma < 4$, there is no solution found except at $\xi = 0$.

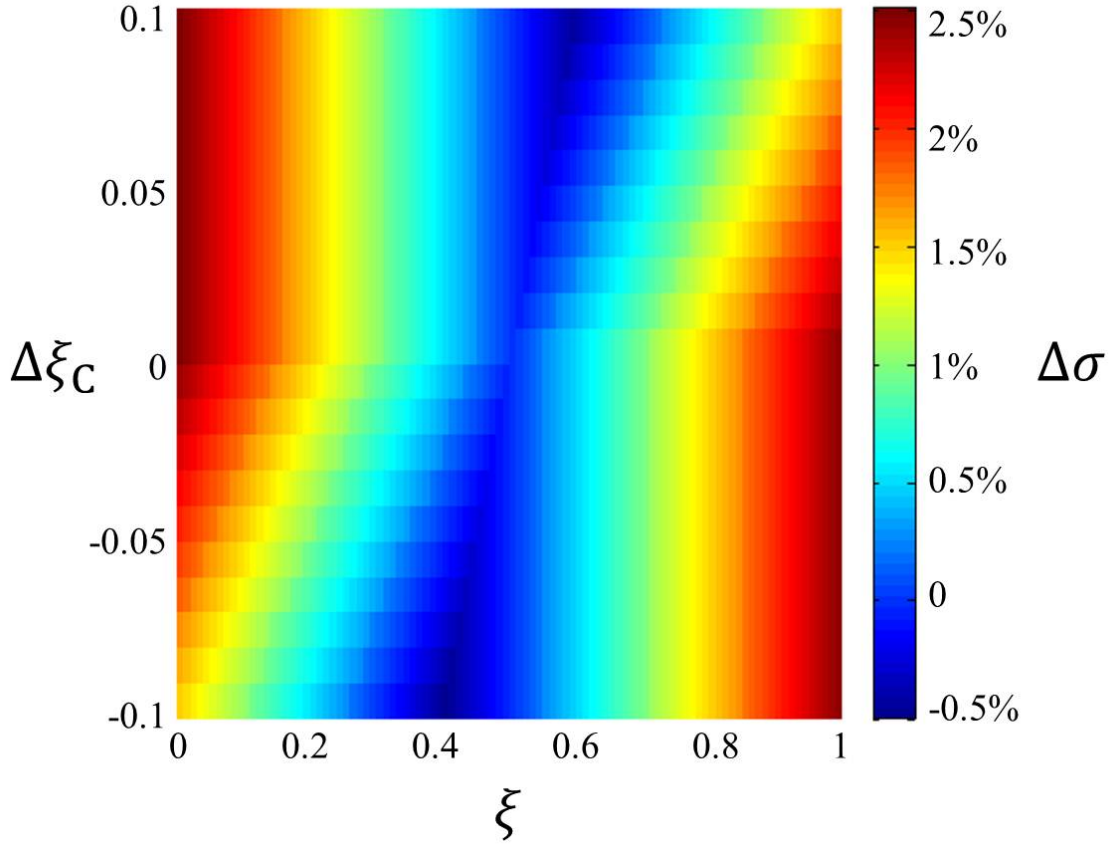

Supplementary Figure 4. Relationship between critical position and morphogen-derived positional error. Shown is a heat map depicting the difference in morphogen-derived positional errors $\Delta\sigma$ between two otherwise-identical systems except a difference in their critical positions, $\Delta\xi_C = \xi_{C2} - \xi_{C1}$. In this analysis, $\Delta\sigma$ is calculated according to Supplementary Eq. 38, thus considering only morphogen-derived positional errors due to imperfect scaling. The fractional variation in embryo length η_L is set at 5% for both systems and ξ_{C1} is set at 0.5 for the first system. See text for further details.

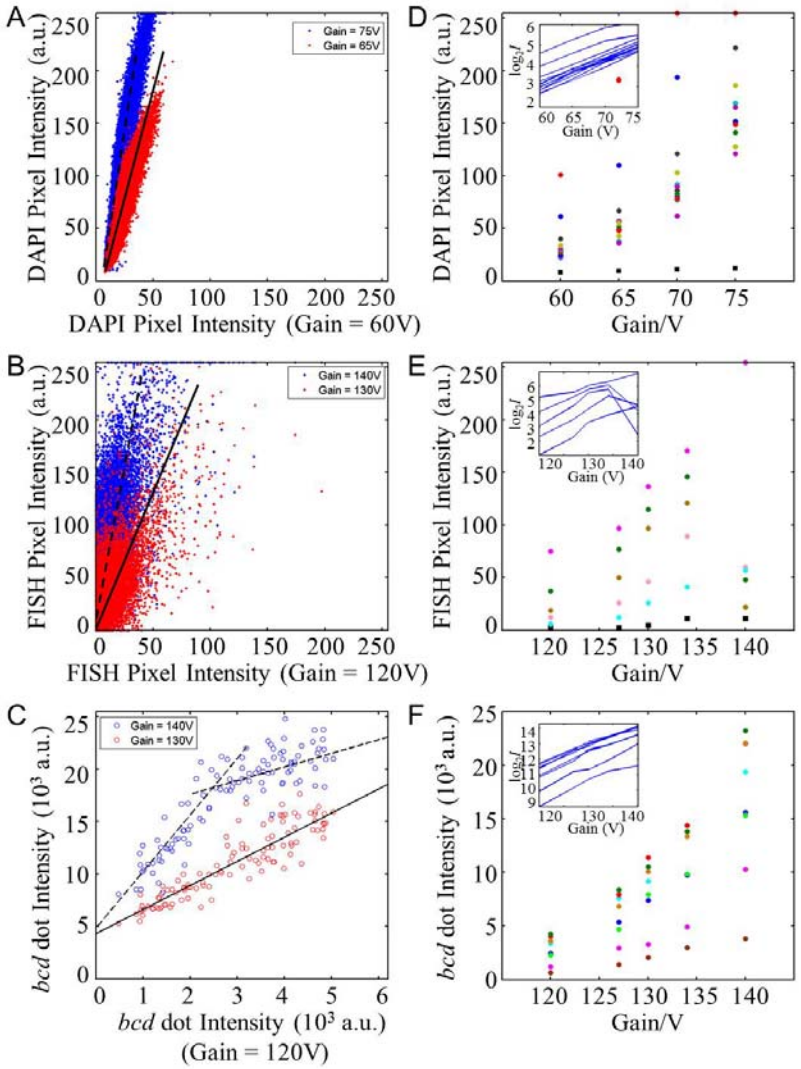

Supplementary Figure 5. Establishing Confocal imaging setting based on documented linearity in signal detection. Scatter plots of pixel intensities of 3 images of the entire DAPI channel (A), pixel intensities of 3 images of the entire *bcd* DNA FISH channel (B) and aggregated intensities of the detected *bcd* DNA FISH dots (C) under different settings of Confocal photomultiplier gain. A linear relationship documents that there is no signal saturation during imaging under the settings tested within the entire signal intensity range analyzed. In (A), blue: $R^2 = 0.99$ for 75V against 60V; red: $R^2 = 0.99$ for 65V against 60V. In (B), blue: $R^2 = 0.94$ for 140V against 120V; red: $R^2 = 0.91$ for 130V against 120V. In (C), blue: $R^2 = 0.84$ for 140V against 120V for data points with an intensity < 300 a.u.; red: $R^2 = 0.89$ for 130V against 120V. Note, for example, the non-linearity in the high intensity range under the setting of 140V gain (panel C, blue), documents the unsuitability of this setting and rules out its use in our experiments. (D-F) Shown are DAPI intensity, *bcd* DNA FISH intensity or aggregated intensities of detected *bcd* DNA FISH dots as a function of gain. Insets represent plots on log2 scale. Acquirements of all experimental data in this study were based on the same chosen microscopic settings with documented linearity: 65V for DAPI and 130V for DNA FISH.

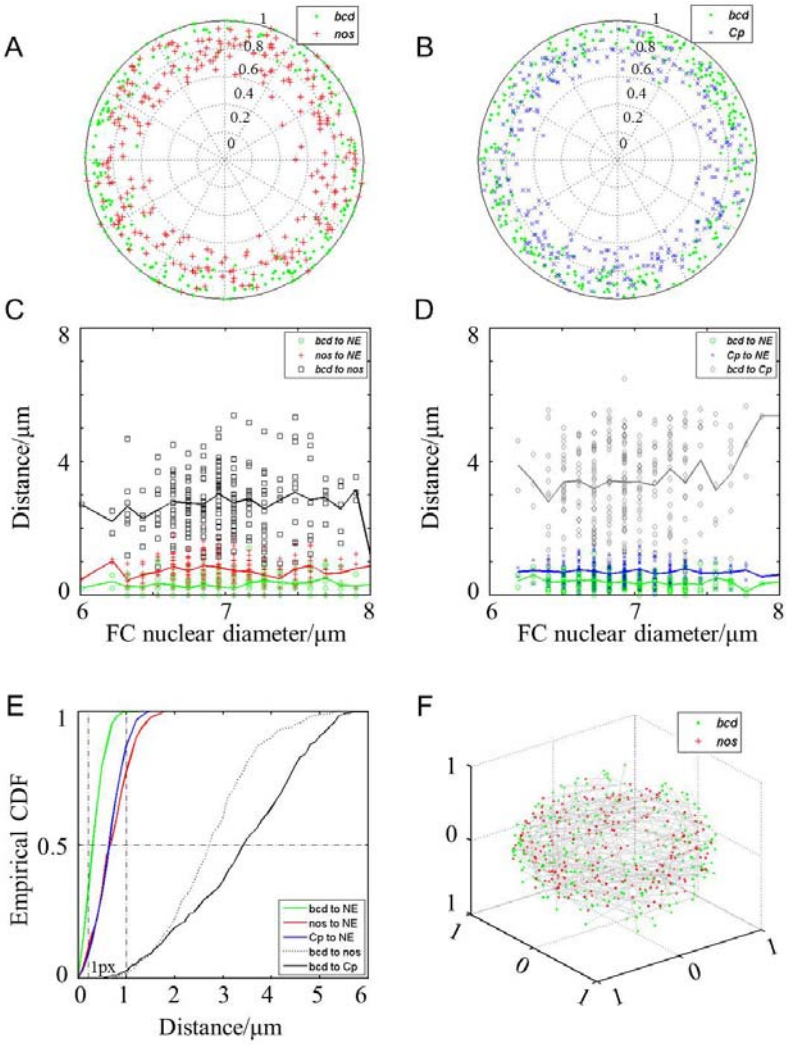

Supplementary Figure 6. A spatial characterization of gene loci in follicle cell nuclei. A-B) 2-D polar plots showing that the *bcd* locus (green dots) is localized more peripherally near the nuclear envelope (NE) than the *nos* (red plus) and *Cp* (blue crosses) loci in the follicle cells. C-D) Plots showing the distances between the *bcd* locus and NE (green), between the *nos* locus and NE (red plus), between the *Cp* locus and NE (blue crosses), between the *bcd* and *nos* loci within the same nucleus (black squares), or between the *bcd* and *Cp* loci within the same nucleus (gray diamonds), as a function of the nuclear diameter of follicle cells. Solid lines represent the average profiles. (E) Shown is an empirical cumulative density function of the 5 distance measurements in panels C and D. The means of these 5 distances are 0.31, 0.74, 0.70, 2.79 and 3.40 µm, respectively. (F) Shown is a 3-D polar plot of the radial distributions of the *bcd* (green dots) and *nos* loci (red plus). Each gray line represents the Euclidean distance between the *bcd* and *nos* loci within a follicle cell nucleus.

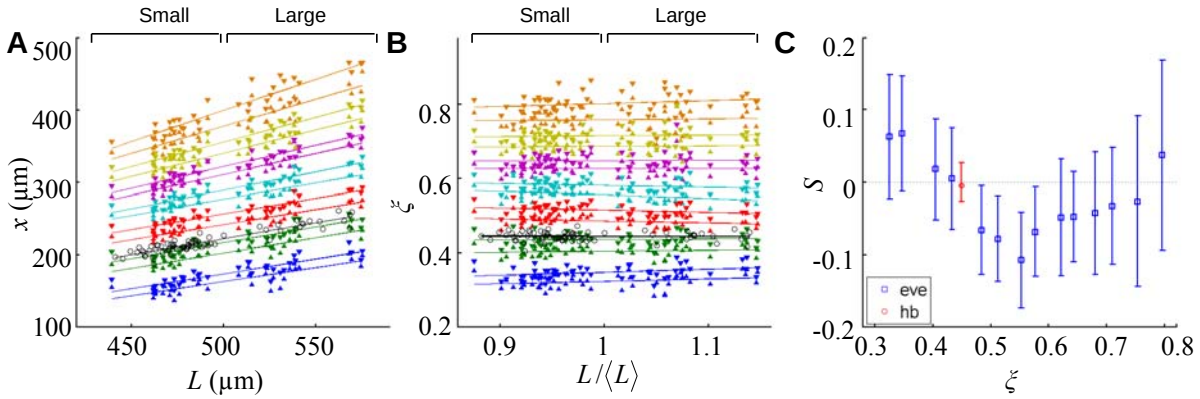

Supplementary Figure 7. Gene expression boundary measurements in embryos. Scatter plot of absolute (A) or relative positions (B) of *hb* (black) or *eve* (colored) expression boundaries in embryos from the large- and small-egg inbred lines. C) The regression slopes of (B) are plotted as a function of relative boundary position. Error bars represent 95% CI of each fitted slope.

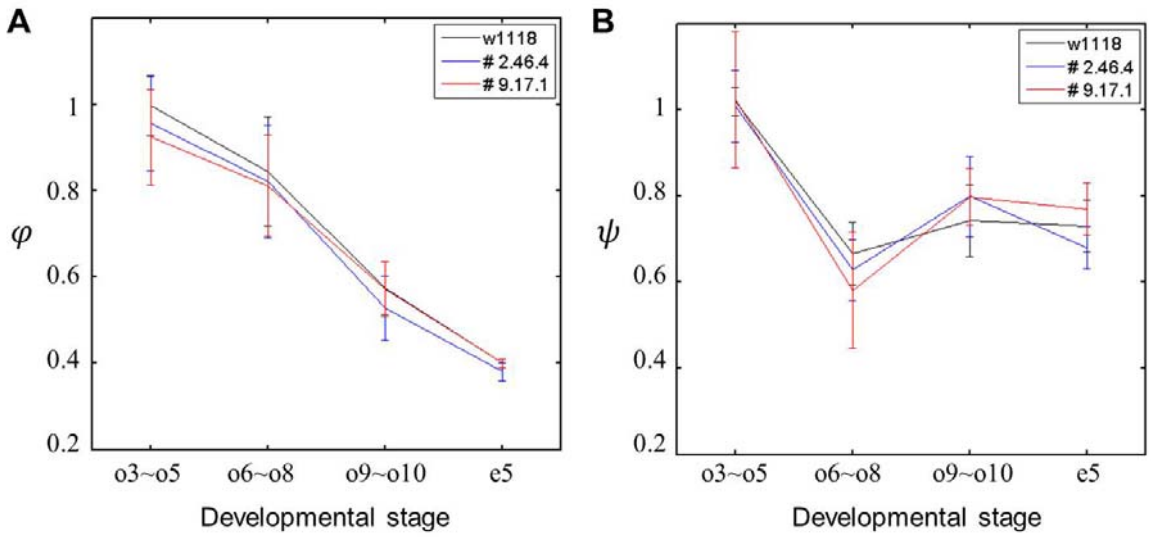

Supplementary Figure 8. Conservation of both 3-D shape and tissue expansion anisotropy among tested *Drosophila* lines. Shown in panels A and B are plots of, respectively, 3-D shape (φ) and expansion anisotropy (ψ) as a function of developmental time. The three *Drosophila* lines examined are as indicated. The developmental times shown represent oogenesis stages 3 to 10A and embryonic stage 5. $\varphi = 1$ denotes a perfectly round shape along the two axes examined; $\psi = 1$ denotes isotropic expansion along the two axes examined (see Supplementary Note 3).

Supplementary Tables

Supplementary Table 1. Primer sequences.

nos (spanning 21.8kb)

Forward Primers	Reverse Primers
TGC TAA TTG GCC GAC AAA CG	TTG CTA AAG GTC ACG CCG AT
GCT TTC ACT GTC GGC TGA GT	CTT TTA GCC CAA GCC AAG CC
TCG CAT AAA CCG CTC ACG AA	GCA GAA TAA GCC GAA CGA GC
GGG CTG CGG AGT AAA GTC AT	TTG CTC TGT GCT TTC GTT GC
GTG CAA CCC CAA TCA CGA CT	GCT CTC TTC TCT CTC CGC AC
TTG TTT CTC TTT CCC GCG CT	TCG CTG AAT AAC AAT GCG TCG
CGA GGT TGT TGA CAC GTT CC	TGC AAA TTC AAG CCG ATG CC

bcd (spanning 16.9kb)

Forward Primers	Reverse Primers
AGC TGT CAC AGA GTC GTG C	GGC GCA TTG TGG TAA AGG TT
CAC CTG CAC ACC CTG TTA CT	CGC AGC ATA TGC AAG TGA CC
TGA AAA GGA TCC TGG CGA CC	GTG TTA GTC CCT CAA CGC CA
ATG GGT AGC CTT TTG GTG GG	TTT CCA CCA GCC CAT CCA TC
GAC TAG CCA AGT CCG ACG AC	CGA ACA CCC GCG GAT CAT AA
GAA CAG TAC GGC AAA GCT GC	CCA GTT CCG CAC AGT GGT AT
GCG ACC CTG AAT GCT GAA TG	TTA TGG CAT GGC GCA CTA CT

Cp (spanning 19.8kb)

Forward Primers	Reverse Primers
AGA AAG TCC TTG CGA CCA GC	ACG TCC AAC TCA TGT GGT CC
TGA TCC CAT GCA ACT GTG CT	ATC GTT GCG CCC CTT AAA GA
AAG GCG GGT CAC ACC TAT TG	TGC GTA CCT TGA GCC CAG TA
TAC TGG GCT CAA GGT ACG CA	AAC TGT TGT GGG TTC TGG GG
GCC AAC TCG GTT GAT CTC TC	ATC GAC GGA GGG TCA TTG TG
TAC CAC ACA ATG ACC CTC CG	TGA CCA CGG CTA ATT GCA GA
ATC GAC CTG GAC CTA GTG CT	GCA CAC ATT GAC TGC CAA CA
CAG TCA ATG TGT GCG GCT ATG	TTG AGC TGA AGA GCC GTC TG

Shown are primer pairs used in generating the probe sets for DNA FISH. All sequences are listed as 5' to 3'.

Supplementary Table 2. Model-based and experimentally estimated parameter values under the TEM^{3}S framework.

	TEM^{3}S-idealized	Measured in #2.46.4 & #9.17.1			Measured in w^{1118}		
		mean	standard deviation		mean	standard deviation	
γ	0	0.60	0.04		0.62	0.07	
Γ	6	6.19	1.04		5.65	0.46	
		exponent	95% CI	R^2	exponent	95% CI	R^2
n_J	3	2.70	2.36~3.04	0.86	2.89	1.86~3.92	0.28
n_D	0	NA	NA	NA	NA	NA	NA
n_Γ	1	0.65	-0.12~1.42	0.74	0.92	-0.27~2.11	0.91
n_γ	0	-0.09	-0.49~0.31	0.02	-0.004	-0.07~0.07	0.0004

Parameters are defined as in Supplementary Information. n_J was estimated using the scaling power of *bcd* mRNA (n_2) measured in freshly-laid eggs. Exponent denotes the fitted slope from log-log plots, with 95% confidence interval and R^2 shown. Analysis for two inbred lines was based on data pooled from embryos that had been treated side by side both experimentally and during imaging. Sources of raw data used in this analysis: *bcd* mRNA FISH and Bcd staining for inbred lines [3], Bcd staining in w^{1118} [ref 1], and *bcd* mRNA FISH in w^{1118} (this study). #2.46.4 & #9.17.1 refer to the large- and small-egg inbred lines, respectively. NA, not available.

Supplementary Table 3. Scaling power values estimated using different size measurements.

Line	n_2		
	$\frac{\mathrm{d}R/R}{\mathrm{d}L/L}$	$\frac{\mathrm{d}R/R}{\mathrm{d}H/H}$	$\frac{\mathrm{d}R/R}{\mathrm{d}\sqrt[3]{LH^2}/\sqrt[3]{LH^2}}$
w^{1118}	2.89 ± 1.03	3.71 ± 1.11	3.45 ± 1.09
2.46.4	2.81 ± 0.32	3.31 ± 0.45	3.14 ± 1.03
9.17.1	2.64 ± 0.31	3.59 ± 0.52	3.30 ± 1.03

Line	n_3		
	$\frac{\mathrm{d}A/A}{\mathrm{d}L/L}$	$\frac{\mathrm{d}A/A}{\mathrm{d}H/H}$	$\frac{\mathrm{d}A/A}{\mathrm{d}\sqrt[3]{LH^2}/\sqrt[3]{LH^2}}$
w^{1118}	3.05 ± 0.92	3.96 ± 0.99	3.67 ± 0.97
2.46.4	3.19 ± 1.05	3.82 ± 0.90	3.68 ± 0.92
9.17.1	2.97 ± 0.98	3.69 ± 0.84	3.39 ± 0.86

Supplementary Notes

Supplementary Note 1. Basic features of the TEM^{3}S model

1.1. An exponential morphogen gradient of patterning system

As detailed in the main text, the TEM^{3}S model states that a morphogen gradient possesses properties to achieve a performance objective of attaining perfect scaling at one (or more) relative position in system **P**,

$$\frac{\partial M(L,\xi,t)}{\partial L} = 0 . \qquad (1)$$

To obtain the analytical solutions of ξ_C, we start with an idealized 1-D model based on synthesis, diffusion and decay (SDD) (Supplementary Eq. 2). Here, morphogen protein molecules, $M(L,\xi,t)$, are synthesized at a constant rate J from a point source at one end (specified by the Heaviside function). The morphogen molecules diffuse from this source (with a diffusion coefficient D) and undergo first-order decay (with a rate constant ω).

$$\frac{\partial M(L,\xi,t)}{\partial t} = \frac{D}{L^2}\frac{\partial^2 M}{\partial \xi^2} - \omega M + J\,\Theta(\xi)\Theta(-\xi) \qquad (2)$$

Given the initial condition of no morphogen protein in system **P** and the no-flux condition except at $\xi = 0$ where $-\frac{D}{L}\frac{\partial M}{\partial \xi} = J$, the analytical solution is

$$M(L,\xi,t) = Ae^{-\Gamma\xi}(1+e^{2\Gamma(\xi-1)})\frac{\operatorname{erfc}(\frac{\Gamma\xi}{2\sqrt{\omega t}} - \sqrt{\omega t}) - e^{2\Gamma\xi}\operatorname{erfc}(\frac{\Gamma\xi}{2\sqrt{\omega t}} + \sqrt{\omega t})}{2}, \qquad (3)$$

and for a sufficiently large Γ, the solution can be simplified as

$$M(L,\xi,t) = Ae^{-\Gamma\xi}\frac{\operatorname{erfc}(\frac{\Gamma\xi}{2\sqrt{\omega t}} - \sqrt{\omega t}) - e^{2\Gamma\xi}\operatorname{erfc}(\frac{\Gamma\xi}{2\sqrt{\omega t}} + \sqrt{\omega t})}{2}, \qquad (4)$$

where

$$A = \frac{J}{\sqrt{D\omega}} \text{ and } \Gamma = \frac{L}{\sqrt{D/\omega}}. \qquad (5)$$

At $t \to \infty$, a steady state is reached and the concentration of morphogen molecules, M_s, is an exponential function of ξ as,

$$M_s(L,\xi) = Ae^{-\Gamma\xi} \qquad (6)$$

In Supplementary Eq. 6, A is the amplitude at $\xi = 0$, and Γ is the absolute slope of $\ln(M_s)$ denoting the patterning system's length in relation to the length scale of the morphogen gradient. We refer to Γ as the system attribute to provide a perspective that underscores a balance between the properties of the patterning system and the morphogen gradient toward achieving a performance objective, a core feature of TEM^{3}S (see Main text and below). When considering a steady-state morphogen gradient, A and Γ are quantities irrespective to space or time, but they both (or either) could be a function of L.

Analytical solutions of the critical position could exist for the above system. For mathematical expression with regard to scaling, we introduce a parameter, scaling power, which

is defined as the normalized derivative of any biological quantity Q with respect to that of the length L of a biological entity,

$$n \equiv \frac{\mathrm{d}Q/Q}{\mathrm{d}L/L}. \tag{S7}$$

If a scaling power n could be approximated to a finite constant value with respect to L, a power-law relationship in the form of $Q \propto L^n$ would be found. n = 0 denotes that the biological quantity is independent of L, while n = 1 denotes that the quantity is linear to L. For an exponential morphogen gradient, we denote the relative derivatives of the quantities J, D and ω in response to changes in L as their respective scaling power: $n_J \equiv \frac{\mathrm{d}J/J}{\mathrm{d}L/L}$, $n_D \equiv \frac{\mathrm{d}D/D}{\mathrm{d}L/L}$ and $n_\omega \equiv \frac{\mathrm{d}\omega/\omega}{\mathrm{d}L/L}$. We also define, in similar ways, the scaling power for compound parameters: $n_A \equiv \frac{\mathrm{d}A/A}{\mathrm{d}L/L}$ and $n_\Gamma \equiv \frac{\mathrm{d}\Gamma/\Gamma}{\mathrm{d}L/L}$. Given these definitions and the steady-state exponential function of the morphogen gradient (Supplementary Eq. 6), we find

$$\frac{\partial M_\mathrm{s}}{\partial L} = \frac{M_\mathrm{s}}{L}(n_A - n_\Gamma \Gamma \xi). \tag{8}$$

Under the condition of $n_A = 0$ and $n_\Gamma = 0$, which denote that both A and Γ are independent of L, $\frac{\partial M_\mathrm{s}}{\partial L} = 0$ at all positions ξ. Under the condition of $n_A \neq 0$ and $n_\Gamma = 0$, there is no position at which $\frac{\partial M_\mathrm{s}}{\partial L} = 0$. When $n_\Gamma \neq 0$, only one critical position solution exists,

$$\xi_\mathrm{C} = \frac{n_A}{\Gamma n_\Gamma}. \tag{9}$$

Supplementary Eq. 9 can be alternatively expressed using the scaling powers of rate constants in the SDD model,

$$\xi_\mathrm{C} = \frac{n_J - \frac{n_D}{2} - \frac{n_\omega}{2}}{\Gamma(1 - \frac{n_D}{2} + \frac{n_\omega}{2})}. \tag{10}$$

In the case of the Bcd morphogen gradient, we assume that, with experimental support [3,5], diffusivity and decay of morphogen molecules are properties intrinsic to a species and thus independent of tissue length ($n_D = n_\omega = 0$), where the scaling power of the gradient's amplitude n_A can be approximated by the scaling power of the production rate n_J ($n_A \approx n_J$) and

$$\xi_\mathrm{C} \approx \frac{n_J}{\Gamma}. \tag{11}$$

Supplementary Eq. 11 shows that, for an exponential gradient of a maternal morphogen, of which neither diffusion nor degradation scales with system length, the performance objective of attaining a critical position can be achieved only if the system attribute Γ and the scaling power n_J of the morphogen gradient are properly balanced with each other.

For a time-dependent gradient as in Supplementary Eq. 4, we find

$$\xi_C(t) = \frac{n_A}{\Gamma n_\Gamma} \frac{\mathrm{erfcx}(\frac{\Gamma\xi_C}{2\sqrt{\omega t}} - \sqrt{\omega t}) - \mathrm{erfcx}(\frac{\Gamma\xi_C}{2\sqrt{\omega t}} + \sqrt{\omega t})}{\mathrm{erfcx}(\frac{\Gamma\xi_C}{2\sqrt{\omega t}} - \sqrt{\omega t}) + \mathrm{erfcx}(\frac{\Gamma\xi_C}{2\sqrt{\omega t}} + \sqrt{\omega t})} + \frac{n_\omega}{\Gamma n_\Gamma} \frac{2\sqrt{\frac{\omega t}{\pi}}}{\mathrm{erfcx}(\frac{\Gamma\xi_C}{2\sqrt{\omega t}} - \sqrt{\omega t}) + \mathrm{erfcx}(\frac{\Gamma\xi_C}{2\sqrt{\omega t}} + \sqrt{\omega t})} \quad (12)$$

Supplementary Eq. 12 specifies a single solution of ξ_C at each time point $t > 0$. Supplementary Eq. 12 becomes Supplementary Eq. 9 when $t \to \infty$. Supplementary Fig. 1 plots the numerical solutions by assuming $n_D = n_\omega = 0$ and ω = 0.05 min^{-1} ref 6. This figure shows that, at t > 120 min, ξ_C approaches a steady-state position that is determined solely by the balance between n_A and Γ. In *Drosophila* embryos, most AP patterning decisions, including *hb* expression, are made around this time [7,8].

1.2. Is there anything special about the mid-point of system ***P****?*

As discussed above, the critical position ξ_C is constrained by the ratio of n_A / Γ. Let's consider an idealized system **P** in which n_J = 3, n_D = 0 and n_ω = 0. In such a system, a theoretical value Γ = 6 would correspond to ξ_C = 0.5. When Γ of this system is changed to either 10 or 3, ξ_C would be shifted to 0.3 or 1.0, respectively. If the critical position actually coincides with the expression boundary of a patterning gene(s) that has essential developmental functions (see Main text), such large shifts caused by the changes in Γ would be biologically unacceptable and would severely disrupt the patterning outcome, i.e., barring a rewiring of the regulatory network, either the essential gene's expression boundary would have to be shifted to these new, drastically different critical positions or its boundary would become no longer scaled when responding to the morphogen input. As documented in Main text based on the postulate presented in Supplementary Note 2, n_A is a quantity that is reflective of, and constrained fundamentally by, the dynamic properties of system **E**. Assuming n_A is a fundamental value that cannot be altered in a significant way (i.e., without causing deleterious effects on its own), allowing ±10% fluctuations in ξ_C = 0.5 would lead to a predicted Γ range of 6.0 ± 1.3. Such a theoretical range of Γ is consistent with our experimental measurements of the Bcd gradient profiles from w^{1118} embryos or pooled from two inbred lines that have embryo size extremes (Supplementary Table 2). Importantly, this value is also consistent with measurements of the Bcd gradient profiles in different dipteran species that have eggs of dramatically different sizes [5], *Lucilia sericata*, *Drosophila melanogaster* and *Drosophila busckii* ($\langle\Gamma\rangle$ = 7.2, 6.5 and 6.3, respectively). Thus, under the fundamental constraint of $n_J \approx 3$, species that have evolved to have dramatically larger or smaller eggs were also under the selection pressure to preserve $\Gamma \approx 6$ (here a predicted value corresponding to $\xi_C \approx 0.5$) to avoid disruptions of the patterning outcome, absent of a rewiring of the regulatory network in system **P**. Thus the TEM^{3}S model also provides a unified framework to explain Bcd gradient scaling mechanisms observed both within a species and across different dipteran species.

Does a patterning system benefit from the choice of ξ_C = 0.5? Here we analyze an idealized system **P** by evaluating the contributions of imperfect scaling derived from the

morphogen gradient at locations that are away from the critical position. According to Eq. 3 in Main text, the root-mean-square error of morphogen-provided positional information as a function of ξ can be expressed as

$$\sigma(\xi) \approx \eta_L \left| \xi_C - \xi \right|, \tag{13}$$

where $\eta_L = \delta L / L$. Integration of the squared error along the length yields the total variation in position information from imperfect scaling of the morphogen gradient as

$$\int_{\xi=0}^{\xi=1} \sigma^2 \, \mathrm{d}\xi = (\xi_C - \frac{1}{2})^2 \eta_L^2 + \frac{\eta_L^2}{12}. \tag{14}$$

Supplementary Eqs. 13 and 14 show that, while the positional error (with respect to scaling) at a given position is a function of its distance from the critical position, the aggregate error of the entire system is determined only by the fractional variation in system length and the critical position. Supplementary Eq. 14 has a minimum value of $0.083\,\eta_L^2$ at $\xi_C = 0.5$. This suggests that, if the morphogen gradient had an instructive role in patterning at all positions (as in an idealized system), the patterning system would benefit from having a critical position at midpoint with the highest overall scaling information derived from the morphogen gradient.

Supplementary Note 2. Dynamic and fundamental origins of the scaling power: A postulate

To establish a dynamic framework, we consider a system of molecules in biological entities in systems **E** and **P**. These molecules represent the fundamental constituents in a chain of linear-forward transitions (gene → mRNA → protein) that is responsible for the production of morphogen protein molecules in system **P**. While specifically formulated for Bcd, the framework discussed here is applicable to other *Drosophila* maternal gradients if their production (both synthesis and gradient formation) does not involve non-linear steps. The quantities of the molecular species in the chain are: copies of the morphogen gene as maternal DNA (*C*), maternally expressed mRNA molecules (*R*) and morphogen protein concentration (*M*). The biological entities under consideration are: the nurse cell nucleus with 1-D size L_1, the egg chamber with size L_2 and the freshly laid egg with size L (see Supplementary Note 3 for a discussion about 3-D size). Under the TEM^{3}S framework, nurse cell nuclei and egg chambers belong to system **E**, while the blastoderm embryo that begins as a freshly laid egg is system **P**. Here molecular species *C* is unique to system **E**, while *M* is unique to system **P**. Only molecular species *R* in the chain can exist in both systems **E** and **P**.

In our model, the start of oogenesis, i.e., stage 1, marks $t = 0$. In our discussions, we use the term developmental time under the definition that it is the time at which system **E** (or system **P**) passes a developmental landmark. Developmental landmarks can be, but do not have to be, experimentally observable morphological structures such as those used to define the stages of the oogenesis (see Methods). The nature of oogenesis requires the definition of two developmental transitions in our model. At t_1, nurse cells inside an egg chamber are depleted with their entire contents "dumped" into the oocyte [9,10], a transition that corresponds to stage 10. At t_2, system **E** ceases to exist and becomes system **P**, a transition that corresponds to the egg being laid.

We use a system of differential equations to describe the chemical reactions and tissue growth in system **E** (which evolves to become system **P** at t_2). Using first-order rate constants for molecule synthesis and decay and tissue expansion, we have

$$\dot{C} = j_1 C, \qquad 0 \le t \le t_1; \tag{15}$$

$$\dot{L}_1 = k_1 L_1, \qquad 0 \le t \le t_1; \tag{16}$$

$$\dot{R} = \begin{cases} j_2 C - \omega_2 R, & 0 \le t \le t_1 \\ -\omega_2 R, & t > t_1 \end{cases}; \tag{17}$$

$$\dot{L}_2 = \begin{cases} k_1 L_2, & 0 \le t \le t_1 \\ k_2 L_2, & t_1 < t \le t_2 \end{cases}; \tag{18}$$

$$\frac{\partial M(\xi,t)}{\partial t} = \frac{D}{L^2}\frac{\partial^2 M}{\partial \xi^2} - \omega M + j_3 R\,\Theta(\xi)\Theta(-\xi), \quad t \ge t_2; \tag{19}$$

$$\dot{L} = 0, \qquad t \ge t_2. \tag{20}$$

Here the left-hand side of each equation denotes a time derivative, with a corresponding rate constant(s) shown on the right-hand side. Note that Supplementary Eq. 19, which is for system **P**, is identical to Supplementary Eq. 2, where $J = j_3 R$. Also note that j_1 here denotes the first-order rate constant for morghogene gene copy number expansion inside nurse cell nuclei, but since the morphogen gene itself is only a negligible part of the entire genome that is undergoing endoreplication, morphogen gene copy number expansion itself *per se* is not responsible for "driving" the expansion of nurse cell nuclei. For system **E** (i.e., $t \le t_2$), the initial conditions are $C = 1$, $R = 0$, $L_1 = l_0$ and $L_2 = L_0$. Analytical solutions for such a system can be found (not shown).

We define dynamic scaling power m_1 and m_2 as time derivatives,

$$m_1(t) \equiv \frac{\mathrm{d}\,C(t)/C(t)}{\mathrm{d}\,L_1(t)/L_1(t)} = \frac{\dot{C}/C}{\dot{L}_1/L_1} = \frac{j_1}{k_1}, \qquad 0 \le t \le t_1; \tag{21}$$

$$m_2(t) \equiv \frac{\mathrm{d}\,R(t)/R(t)}{\mathrm{d}\,L_2(t)/L_2(t)} = \frac{\dot{R}/R}{\dot{L}_2/L_2} = \begin{cases} \dfrac{j_1 - \omega_2 + (j_1 + \omega_2)\coth(\frac{j_1+\omega_2}{2}t)}{2k_1}, & 0 \le t \le t_1 \\ -\dfrac{\omega_2}{k_2}, & t_1 < t \le t_2 \end{cases}; \tag{22}$$

For a sufficiently large t prior to t_1, $\coth(\frac{j_1+\omega_2}{2}t)$ approaches 1, which leads m_2 to converge with m_1 at $\frac{j_1}{k_1}$. In an idealized system, 6 rounds of endoreplication will result in m_2 to differ from m_1 by less than 5% ($\coth(\frac{j_1+\omega_2}{2}t) \approx 1.03$). In other words, $\frac{j_1}{k_1}$ is the fundamental definition for the dynamic scaling power of both C and R in system **E** prior to t_1. Between t_1 and t_2, nurse cells do not exist in our model and, thus, there is no transcription that is relevant to morphogen production in the future system **P**. During this period, there is continued growth of the egg chamber, which we refer to as the "empty growth" period because it has a negative or close to zero (if $\omega_2 \approx 0$) scaling power m_2 in absolute terms whereas m_1 no longer exists.

We now consider discrete experimental measurements by adapting the continuous definitions through the use of integration

$$n_1 \equiv \frac{\int_C^{C+\delta C} \frac{\mathrm{d}C}{C}}{\int_{L_1}^{L_1+\delta L_1} \frac{\mathrm{d}L_1}{L_1}} = \frac{\ln(1+\frac{\delta C}{\langle C \rangle})}{\ln(1+\frac{\delta L_1}{\langle L_1 \rangle})}, \tag{23}$$

where δL_1 denotes the variation in nurse cell nuclear size under experimental evaluations and δC denotes the part of variation in maternal DNA copy number due to δL_1. According to Supplementary Eq. 23, n_1 can be estimated by the fitted slope of a log-log plot (Main Fig. 3). Thus n_1 obtained from our experimental data effectively measures the average dynamic scaling power of gene copies during the relevant period of developmental time (see Main text).

We can also use a similar integration approach toward estimating the scaling power of R based on experimental measurements made in freshly laid eggs, where the transition from system **E** and system **P** has just taken place,

$$n_2 \equiv \frac{\int_R^{R+\delta R} \frac{\mathrm{d}R}{R}}{\int_L^{L+\delta L} \frac{\mathrm{d}L}{L}} = \frac{\ln(1+\frac{\delta R}{\langle R \rangle})}{\ln(1+\frac{\delta L}{\langle L \rangle})}, \tag{24}$$

Here δR represents the part of variation in maternally expressed mRNA molecule number due to embryo-to-embryo size fluctuations δL. Since n_2 is measured from system **P**, $L = L_2(t_2)$ and $R \approx R(t_2)$. Let developmental time be the only source of variation. Then the variations in L and R can be analytically estimated to first order of the variation in time. Considering the developmental transition at t_1 for system **E**, we have

$$n_2 \approx \frac{\ln(1+\frac{\left|\dot{R}(0 \le t \le t_1)\right|\delta t_1 + \left|\dot{R}(t_1 < t \le t_2)\right|\delta t_2}{\langle R \rangle})}{\ln(1+\frac{\left|\dot{L}_2(0 \le t \le t_1)\right|\delta t_1 + \left|\dot{L}_2(t_1 < t \le t_2)\right|\delta t_2}{\langle L \rangle})} \approx \frac{j_1 \delta t_1 + \omega_2 \delta t_2}{k_1 \delta t_1 + k_2 \delta t_2}, \tag{25}$$

where δt_1 and δt_2 denote developmental time variations for each of the two phases of oogenesis, from 0 to t_1 and from t_1 to t_2, respectively. Let $\frac{\delta t_1}{t_1} = \frac{\delta t_2}{t_2 - t_1}$, which means a steady progression in development, and we have

$$n_2 \approx \frac{j_1 + \omega_2 \frac{t_2 - t_1}{t_1}}{k_1 + k_2 \frac{t_2 - t_1}{t_1}}. \tag{26}$$

Based on experimental observations (see Main Fig. 1b), we know $k_2 \approx k_1$ and $\frac{t_2 - t_1}{t_1} \approx 0.1$. In addition, it is well documented that maternal mRNA molecules in oocytes and early embryos are very stable [11]. Under these conditions the impact of the "empty growth" period on the scaling power n_2 becomes negligible when considering the entire duration of system **E** (although as noted above it can directly impact the dynamic scaling power m_2 of system **E** during this period). Thus, n_2, which is calculated from experimental measurements made in freshly laid eggs, can also be approximated by $\frac{j_1}{k_1}$, the fundamental definition of the dynamic scaling power for both the *bcd* gene template number and *bcd* mRNA molecule number. In other words, n_2 in system **P** is set fundamentally by the dynamic properties of system **E**.

Similarly, we define the scaling power of morphogen gradient's amplitude in system **P** for discrete measurements as

$$n_3 \equiv \frac{\int_A^{A+\delta A} \frac{\mathrm{d}A}{A}}{\int_L^{L+\delta L} \frac{\mathrm{d}L}{L}} = \frac{\ln(1+\frac{\delta A}{\langle A \rangle})}{\ln(1+\frac{\delta L}{\langle L \rangle})}, \tag{27}$$

where δA is the part of variation in morphogen gradient amplitude due to embryo-to-embryo size fluctuations δL. Experimentally, n_3 is the estimated slope of the linear regression, $\ln(A/\langle A \rangle)$ vs. $\ln(L/\langle L \rangle)$. As shown in Supplementary Note 1, subsection 1.1, $A = \frac{j_3 R}{\sqrt{D\omega}}$. Assuming that all three rate constants, j_3, D and ω, are independent of either time or L, we obtain analytically, $\frac{\delta A}{\langle A \rangle} \sim \frac{\delta R}{\langle R \rangle}$ and $n_3 \sim n_2$. Importantly, when the relationship between $\ln(A/\langle A \rangle)$ and $\ln(L/\langle L \rangle)$ is close to linear, n_3 represents a direct experimental approximation of n_A.

In summary, our analyses described in this section document a chain rule of scaling,

$$n_A \sim n_3 \sim n_2 \sim n_1 \approx \frac{j_1}{k_1}, \tag{28}$$

where the scaling power of the morphogen gradient's amplitude n_A in system **P** is determined fundamentally by the dynamic properties of system **E** and can be estimated by independent means under the framework of our experimental approaches. In Main text, we refer to Supplementary Eq. 28 as the postulate about the fundamental connection between systems **E** and **P**. This postulate thus not only unifies two distinct stages of a life cycle but also imposes specific limitations on how a developmental program under temporal logic **c** can be constructed at a fundamental level (see Main text and Supplementary Note 1). Our estimates of n_1, n_2 and n_3 can all be approximated by ~3, suggesting that the first-order rate constants j_1 and k_1 are related to each other by a ratio of ~3. This supports a model where *bcd* gene template expansion (i.e., DNA replication for nurse cell-expressing genes) is an event coupled to the expansion of the nurse cell nuclear volume, consistent with the existence of regulatory mechanisms controlling endoreplication [12-14]; see Main text and Supplementary Note 3 (below) for additional discussions.

Supplementary Note 3. Experimental considerations of 3-D shape and expansion anisotropy

This section concerns 3-D shape of biological entities and experimental evaluations of linear dimensions. For a group of nurse cell nuclei at a given stage, we define shape (φ) and expansion anisotropy (ψ) as

$$\varphi \equiv \frac{l_y}{l_x} \text{ and } \psi \equiv \frac{\mathrm{d}\, l_y / l_y}{\mathrm{d}\, l_x / l_x}, \tag{29}$$

where l_x and l_y are experimentally measured diameters. In our study, we used two independent methods to measure l_x and l_y and our conclusions are robust to measurement methods. In one method, we measured l_x and l_y along a randomly chosen axis x and its perpendicular axis y. In a second method, we measured l_x along the AP axis of the egg and l_y along the perpendicular axis. Expansion anisotropy ψ was estimated from experimental data as the fitted slope of a log-log plot. At each stage of oogenesis between stage 3 to stage 10A, we found that both φ and ψ were close to 1 in w^{1118}, large-egg line #2.46.4, and small-egg line #9.17.1. In particular, for nurse cell nuclei at stage 10A in w^{1118}, we obtained $\varphi = 1.05 \pm 0.02$ and $\psi = 1.03 \pm 0.06$ using randomly chosen axes, and $\varphi = 1.02 \pm 0.12$ and $\psi = 0.93 \pm 0.26$ using AP as x axis (standard deviations of ψ were calculated by bootstrapping). These results support a volumetric expansion of nurse cell nuclei. In our analysis of experimental data, we obtained values of scaling power n_0 and n_1 based on two size measurements, and we found them to be robust to measurement methods (data not shown).

Similarly, for a group of egg chambers at a given stage of oogenesis (system **E**) or a group of embryos (system **P**), we define tissue shape (φ) and expansion anisotropy (ψ) as

$$\varphi \equiv \frac{H}{L} \text{ and } \psi \equiv \frac{\mathrm{d}\, H / H}{\mathrm{d}\, L / L}, \tag{30}$$

where L denotes the 1-D size along the A-P axis and H denotes the 1-D size perpendicular to the A-P axis. At early stages of oogenesis, the observed 3-D shape of egg chambers is approximately spheroid and the expansion is nearly isotropic ($\varphi \approx 1$). After stage 6 of oogenesis, the observed 3-D shape becomes progressively elongated with the expansion along the A-P axis exceeding that along the perpendicular axis (Supplementary Fig. 8), i.e., $\varphi < 1$. An anisotropic expansion of $\psi < 1$ is predicted to lead to higher scaling power n_2 and n_3 when the 1-D embryo size is measured as H or calculated from a spheroid volume ($\sqrt[3]{\pi L H^2 / 6}$) than when the 1-D size is measured directly as L assuming isotropy. To evaluate the potential impact of anisotropic expansion on our estimates of scaling power, we deployed different ways of obtaining the 1-D size, which permitted cross comparisons between our experimental estimates. Supplementary Table 3 lists the estimated values of n_2 and n_3 using different methods of obtaining the 1-D size of the biological entities. Our results show that a consideration of expansion anisotropy did not have a dramatic impact on scaling power measurements in our experimental system to the extent that it would alter our conclusion that n_A has a finite value, independent estimations of which congregate to a cubic power as an overall consensus (Main Fig. 5a).

Supplementary Note 4. Special considerations of the TEM^{3}S model

4.1. Scaling in discrete populations

The concept of a critical position in a patterning system has been postulated when evaluating scaling properties of two average morphogen gradient profiles of two populations [15]. Here, the performance objective can be defined as $M_1 = M_2$ at the critical position ξ_C, or

$$A_1 e^{-\Gamma_1 \xi_C} = A_2 e^{-\Gamma_2 \xi_C}. \quad (31)$$

The critical position solution is found as

$$\xi_C = \frac{\ln(1+\eta_A)}{\Gamma_1 \eta_L}, \quad (32)$$

where $\eta_A = \frac{A_2 - A_1}{A_1}$ and $\eta_L = \frac{L_2 - L_1}{L_1}$.

We adapt this analysis to an idealized system in a discrete population. In this case, the performance objective can be defined as $\frac{\delta M}{\delta L} = 0$ at the critical position, and the scaling power for a morphogen gradient's amplitude in a discrete population is defined by integration of Supplementary Eq. 7 such that,

$$n_A = \frac{\ln(1+\eta_A)}{\ln(1+\eta_L)}, \quad (33)$$

where $\eta_A = \frac{\delta A}{A}$ and $\eta_L = \frac{\delta L}{L}$. It should be noted that our discussions here are about an idealized system where the variations δM and δA are specific to scaling. We are not using Supplementary Eq. 33 to directly analyze experimental data (see Main text), but rather we are using it to identify model-based properties that can be compared with those of real biological systems where additional sources of variations would exist. Under the condition of $n_\Gamma = 1$ in our idealized system in a discrete population, integration of Supplementary Eq. 9 yields the critical position solution,

$$\xi_C = \xi_0 \frac{\ln(1+\eta_L)}{\eta_L} \quad (34)$$

where $\xi_0 = \frac{n_A}{\langle \Gamma \rangle}$. Note that when η_L approaches 0, $\frac{\ln(1+\eta_L)}{\eta_L}$ has an upper bound of 1 and, thus, ξ_C has an upper bound of ξ_0.

Supplementary Fig. 2 plots the relationship (solid lines) between the parameters $\langle \Gamma \rangle$ and η_L predicted by Supplementary Eq. 34 assuming $\xi_C = 0.5$. The relationship depicted here represents what is expected of an idealized system in a discrete population. On this plot, we now display the experimentally observed values derived from real biological systems, including standard lab lines with nominal *L* variations (red) or enhanced *L* variations derived from the divergent egg sizes of inbred lines (green and blue). We can see readily that all of these experimental datapoints fall within the model-predicted band generated by the chosen limits of $n_A = 3$ and 2.7. This analysis shows that, despite the inherent complexities of real biological systems, our TEM^{3}S model provides a conceptual framework that can adequately capture their properties relevant to morphogen gradient scaling. In this context, we note that measurement

errors inherent to experimental detection of an exponential gradient, combined with the existence of additional biological noise, can complicate or obscure a direct and accurate visualization of ξ_C. Thus the properties predicted by our model represent conceptual yardsticks against which experimental data can be evaluated. In addition, analysis of target gene expression boundaries, which tends to be less prone to measurement errors (than analysis of an exponential gradient), can be used as independent methods for cross validations or experimental evaluations (see Main text and Main Fig. 5).

4.2. A system with a finite size of production source

If the production source in a 1-D SDD model has a finite size [0 s], as opposed to a point source, the gradient system can be expressed as,

$$\frac{\partial M(\xi,L,t)}{\partial t} = \frac{D}{L^2}\frac{\partial^2 M}{\partial \xi^2} - \omega M + \frac{J\,\Theta(\xi L)\Theta(s-\xi L)}{s}. \qquad (35)$$

Supplementary Eq. 35 yields a modified steady-state solution including the source region [16],

$$M(\xi) = \begin{cases} \frac{A}{\gamma}(1-e^{-\gamma}\cosh(\Gamma\xi)), & 0 \le \xi \le \frac{\gamma}{\Gamma} \\ \frac{A}{\gamma}\sinh(\gamma)e^{-\Gamma\xi}, & \frac{\gamma}{\Gamma} \le \xi \le 1 \end{cases}, \qquad (36)$$

where A and Γ are defined in the same way as in Supplementary Eq. 5, and $\gamma = \frac{\Gamma s}{L}$.

Within the source region, $0 \le \xi \le \frac{\gamma}{\Gamma}$, no explicit algebraic solution of the critical position could be found. We solved it numerically by varying the 5 necessary parameters, $\Gamma, \gamma, n_A, n_\Gamma$ and n_γ, over several orders of magnitude. 732,050 parameter sets were assayed in total, with 16.5% of them found to have a single solution (not shown). However, given the experimental estimates for the Bcd gradient such as $\Gamma \approx 6$, $n_A \approx 3$ and $n_\Gamma \approx 1$ as discussed in Main text and Supplementary Note 1, a very strong scaling power of n_γ is required to attain a critical position within the source region (Supplementary Fig. 3). Experimental measurements provide a realistic estimate of $\gamma \approx 0.6$ (i.e, $s \approx 0.1L$; see below). When this and the other realistic estimates were used together in our analysis, we obtained no critical position solution for the modified gradient within the source region.

Outside the source region, $\frac{\gamma}{\Gamma} \le \xi \le 1$, a single analytical solution exists under the condition of $n_\Gamma \neq 0$ as

$$\xi_C = \xi_0\left(1 + \frac{n_\gamma}{n_A}(\gamma\coth(\gamma) - 1)\right), \qquad (37)$$

where $\xi_0 = \frac{n_A}{\Gamma n_\Gamma}$. Supplementary Eq. 37 shows that, under the condition of $n_\gamma = 0$ (i.e., γ is not scaled with L), the critical position is insensitive to the source region and remains at ξ_0. If n_γ is a positive value suggesting a degree of scaling of γ with L, we have $\xi_C > \xi_0$, indicting a shift of the critical position away from the source (note that n_A is a positive value for realistic systems under the TEM^{3}S framework). Supplementary Eq. 37 also shows that, as γ approaches 0, the term $\gamma \coth(\gamma) - 1$ approaches 0 and, thus, ξ_C approaches ξ_0. This is the critical position of a point-source system.

4.3. Source size and precision of morphogen-provided positional information

Since source size can affect ξ_C (Supplementary Eq. 37) and, additionally, since ξ_C can affect the precision of morphogen-provided positional information at a given location (Supplementary Eq. 13), a relationship between source size and morphogen-derived positional error (with regard to scaling) can be established by combining these two equations. For two otherwise-identical systems that differ only in source size properties, morphogen-derived positional errors at a given location ξ can be compared with one another, $\Delta\sigma(\xi) = \sigma_2(\xi) - \sigma_1(\xi)$. Applying Supplementary Eq. 13, we obtain

$$\Delta\sigma(\xi) = \eta_L(|\xi_{C1} + \Delta\xi_C - \xi| - |\xi_{C1} - \xi|), \qquad (38)$$

where ξ_{C1} denotes the critical position of the first morphogen system, and $\Delta\xi_C = \xi_{C2} - \xi_{C1}$ denotes the shift of critical position in the second morphogen system relative to the first. Supplementary Fig. 4 plots $\Delta\sigma$ as a function of ξ and $\Delta\xi_C$ using $\xi_{C1} = 0.5$ and $\eta_L = 5\%$. The results reveal a band of locations (on either side to ξ_{C1}) that is "buffered" or robust against $\Delta\xi_C$ in terms of precision of morphogen-derived positional information, as illustrated by a zone that is colored in blue. Within this "buffered" zone, $\Delta\sigma$ is small or could even be negative (a negative $\Delta\sigma$ simply indicates that the positional error derived from the second gradient is smaller at or near ξ_{C2} than that derived from the first gradient at these locations). Outside this "buffered" zone, i.e., at locations further away from ξ_{C1}, $\Delta\sigma$ caused by $\Delta\xi_C$ becomes larger, as illustrated by the increasing warmth of the color. An anterior shift of ξ_{C2} (relative to ξ_{C1}) impacts negatively on precision more preferentially at locations toward the posterior end, and vice versa (see the dark red regions in Supplementary Fig. 4).

Are there examples of a potential connection between source size and patterning precision? Here we consider two sets of experimental data [1,4] where the positions of *hb* expression boundary (as protein or mRNA) and Bcd gradient profiles had each been obtained on a side-by-side basis to permit limited comparisons. These two sets of data are used for our considerations here because each of them has a "mutant" situation leading to an enlarged *bcd* mRNA distribution in the anterior of the embryo, i.e., a larger source size. In both cases, the *hb* boundary position becomes more variable ($\Delta\sigma_{hb} = 1.4\%$ for *stau* mutant relative to w^{1118} in one case, and $\Delta\sigma_{hb} = 1\%$ for a selected "mutant" inbred line relative to its counterpart in the other case). We found that in each of the "mutant" situations, both γ and n_γ are increased [$\gamma = 0.81 \pm$

0.35 and 0.83 ± 0.12; n_γ = 2.70 ± 2.08 and 1.95 ± 0.38; γ was inferred from the AP position at which maximal Bcd concentration was found (*stau* embryos) or estimated by *bcd* mRNA distribution (the "mutant" inbred line)]. These new calculations made under our current framework would forecast posterior shifts of the critical position $\Delta\xi_C$ = 0.10 and 0.07, respectively. Such ξ_C shifts would predict an increase in morphogen-derived positional error (at the observed *hb* boundary location) by $\Delta\sigma_{hb}$ = 0.5% and 0.4%, respectively, which can account for ~40% of the observed increases in boundary variation in each case. Thus these results are consistent with, but they do not prove directly, our theoretical prediction that source size can have a negative impact on patterning precision.

4.4. Scaling power of a power-law gradient

A power-law morphogen gradient has been shown to possess a property of reducing the impact of fluctuations in morphogen production rate [17,18]. Here we perform a limited analysis to evaluate properties of such a gradient specifically in relation to our TEM^{3}S framework. A power-law morphogen gradient can be expressed as

$$M(\xi, L) = \frac{A}{(1+\mu\xi)^\nu}. \tag{39}$$

Assuming the parameters A and μ, but not the exponent ν, as a function of L, the critical position solution for this gradient can be found as

$$\xi_C = \frac{n_A}{\mu(\nu n_\mu - n_A)} \text{ for } n_A \neq \nu n_\mu, \tag{40}$$

where n_A and n_μ are the scaling powers of the quantities A and μ, respectively.

A power-law gradient can be expected if the degradation of the morphogen molecules is nonlinear as

$$\frac{\partial M(L,\xi,t)}{\partial t} = \frac{D}{L^2}\frac{\partial^2 M}{\partial \xi^2} - \omega M^\tau + J\,\Theta(\xi)\Theta(-\xi), \tag{41}$$

where $\tau \neq 1$. When $\tau \neq 1$ and $\tau \neq 3$, a steady-state solution can be found as Supplementary Eq. 39 such that

$$A = \frac{JL}{D\mu\nu},\ \mu = \left(\frac{D^\tau \nu^\tau(\nu+1)}{J^{\tau-1}L^2\omega}\right)^{\frac{1}{\tau-3}} \text{ and } \nu = \frac{2}{\tau-1}. \tag{42}$$

Thus, the scaling power n_A for this power-law gradient is

$$n_A = \left(2+\frac{2}{\tau-3}\right)n_J - \left(2+\frac{3}{\tau-3}\right)n_D + \frac{1}{\tau-3}n_\omega + \frac{\tau-1}{\tau-3}. \tag{43}$$

To evaluate a power-law gradient under the TEM^{3}S framework, we will make assumptions similar to those made for the exponential gradient. In particular, we assume that diffusion and degradation are species-specific properties that are independent of tissue length within a species ($n_D = n_\omega = 0$), and that the morphogen production rate is volumetric ($n_J = 3$) under temporal logic **c**. We obtain

$$n_A = 7 + \frac{8}{\tau-3}. \tag{44}$$

We can see that in terms of scaling power, the linear degradation ($\tau = 1$) can be unified into Supplementary Eqs. 43-44. When $\tau = 3$, the solution cannot be unified into Supplementary Eqs. 42-44, because A and μ are not separable in integration. Under conditions of $\tau \neq 1$ and $\tau \neq 3$, we find $A = \frac{JL}{D\mu}$, $\mu = 2^{-\frac{1}{4}} J^{\frac{1}{2}} D^{-\frac{3}{4}} \omega^{\frac{1}{4}} L$ and $\nu = 1$, leading to the scaling power

$$n_A = \frac{1}{2} n_J - \frac{1}{4} n_D - \frac{1}{4} n_\omega . \tag{45}$$

For $n_D = n_\omega = 0$ and $n_J = 3$, we find $n_A = 1.5$.

To summarize for this part, we obtain the following scaling power n_A for a power-law morphogen gradient under consideration

$$\begin{aligned} &3 < n_A < 7 \text{ when } \tau < 1; \\ &n_A = 3 \text{ when } \tau = 1; \\ &n_A < 3 \text{ when } 1 < \tau < 3; \\ &n_A = 1.5 \text{ when } \tau = 3; \\ &n_A > 7 \text{ when } \tau > 3; \end{aligned} \tag{46}$$

Thus, under our framework, non-linear degradation is expected to decrease the scaling power n_A when $1 < \tau < 3$. A power-law gradient of Bcd was found in embryos lacking the Bcd-interacting co-factor dCBP (*Drosophila* CREB-binding protein) [19]. The reported estimate of τ = 1.74 in such embryos would be expected to provide the morphogen gradient with a very weak scaling power of n_A = 0.65 based on Supplementary Eq. 44, a values that is within the range of measured n_A = 0.01 ± 0.96 (R^2 = 0.001). According to Supplementary Eq. 40, such a weak scaling power predicts a critical position very close to the anterior of the embryo. Based on experimentally measured parameters, we find ξ_C = 0.0002, suggesting a nearly complete loss of scaling for the Bcd gradient in the mutant embryos.

We can calculate the positional error (specific to scaling) derived from a power-law gradient under the framework of a critical position,

$$\sigma(\xi) = \eta_L (n_\mu - \frac{n_A}{\nu}) \left| \xi_C - \xi \right| . \tag{47}$$

If $n_D = n_\omega = 0$, $n_J = 3$ and $\xi_C \approx 0$, Supplementary Eq. 47 becomes

$$\sigma(\xi) \approx \frac{7\tau - 2}{6 - 2\tau} \eta_L \xi , \tag{48}$$

where $1 < \tau < 3$. Supplementary Eq. 48 suggests that, when nonlinear degradation of morphogen molecules has a power between 1 and 3 such as Bcd in embryos lacking dCBP, the scaling-specific positional error derived from the morphogen gradient increases progressively toward the posterior with the mid-embryo being no longer the most precise region with regard to scaling. This could be a contributing factor to the increased variation in *hb* expression boundary in embryos lacking dCBP [19]. In particular, Supplementary Eq. 48 predicts that σ = 8.6% at the observed *hb* boundary position of ξ_{hb} = 0.43. The experimentally observed *hb* boundary position in the mutant embryos is indeed more variable than in w^{1118} embryos (σ = 2.3% and 1.6%,

respectively) although not quite reaching the extreme predicted by our current model. These results suggest that, although further studies are needed, the TEM^{3}S framework and the concept of a critical position can produce potentially useful conceptual forecasts against which experimentally observed biological properties can be evaluated.

Supplementary References

1 He, F. *et al.* Probing intrinsic properties of a robust morphogen gradient in Drosophila. *Developmental cell* **15**, 558-567, doi:10.1016/j.devcel.2008.09.004 (2008).

2 He, F. *et al.* Distance measurements via the morphogen gradient of Bicoid in Drosophila embryos. *BMC developmental biology* **10**, 80, doi:10.1186/1471-213X-10-80 (2010).

3 Cheung, D., Miles, C., Kreitman, M. & Ma, J. Scaling of the Bicoid morphogen gradient by a volume-dependent production rate. *Development* **138**, 2741-2749, doi:10.1242/dev.064402 (2011).

4 Cheung, D., Miles, C., Kreitman, M. & Ma, J. Adaptation of the length scale and amplitude of the Bicoid gradient profile to achieve robust patterning in abnormally large Drosophila melanogaster embryos. *Development* **141**, 124-135, doi:10.1242/dev.098640 (2014).

5 Gregor, T., Bialek, W., de Ruyter van Steveninck, R. R., Tank, D. W. & Wieschaus, E. F. Diffusion and scaling during early embryonic pattern formation. *Proceedings of the National Academy of Sciences of the United States of America* **102**, 18403-18407, doi:10.1073/pnas.0509483102 (2005).

6 Liu, J., He, F. & Ma, J. Morphogen gradient formation and action: insights from studying Bicoid protein degradation. *Fly* **5**, 242-246 (2011).

7 Fowlkes, C. C. *et al.* A quantitative spatiotemporal atlas of gene expression in the Drosophila blastoderm. *Cell* **133**, 364-374, doi:10.1016/j.cell.2008.01.053 (2008).

8 Surkova, S. *et al.* Characterization of the Drosophila segment determination morphome. *Developmental biology* **313**, 844-862, doi:10.1016/j.ydbio.2007.10.037 (2008).

9 Buszczak, M. & Cooley, L. Eggs to die for: cell death during Drosophila oogenesis. *Cell death and differentiation* **7**, 1071-1074, doi:10.1038/sj.cdd.4400755 (2000).

10 Weil, T. T., Forrest, K. M. & Gavis, E. R. Localization of bicoid mRNA in late oocytes is maintained by continual active transport. *Developmental cell* **11**, 251-262, doi:10.1016/j.devcel.2006.06.006 (2006).

11 Surdej, P. & Jacobs-Lorena, M. Developmental regulation of bicoid mRNA stability is mediated by the first 43 nucleotides of the 3' untranslated region. *Molecular and cellular biology* **18**, 2892-2900 (1998).

12 de Nooij, J. C., Graber, K. H. & Hariharan, I. K. Expression of the cyclin-dependent kinase inhibitor Dacapo is regulated by cyclin E. *Mechanisms of development* **97**, 73-83 (2000).

13 Edgar, B. A. & Orr-Weaver, T. L. Endoreplication cell cycles: more for less. *Cell* **105**, 297-306 (2001).

14 Calvi, B. R., Lilly, M. A. & Spradling, A. C. Cell cycle control of chorion gene amplification. *Genes & development* **12**, 734-744 (1998).

15 Umulis, D. M. & Othmer, H. G. Mechanisms of scaling in pattern formation. *Development* **140**, 4830-4843, doi:10.1242/dev.100511 (2013).

16 Dalessi, S., Neves, A. & Bergmann, S. Modeling morphogen gradient formation from arbitrary realistically shaped sources. *Journal of theoretical biology* **294**, 130-138, doi:10.1016/j.jtbi.2011.10.014 (2012).

17 Eldar, A. *et al.* Robustness of the BMP morphogen gradient in Drosophila embryonic patterning. *Nature* **419**, 304-308, doi:10.1038/nature01061 (2002).

18 Saunders, T. E. & Howard, M. Morphogen profiles can be optimized to buffer against noise. *Physical review. E, Statistical, nonlinear, and soft matter physics* **80**, 041902 (2009).
19 He, F. *et al.* Shaping a morphogen gradient for positional precision. *Biophysical journal* **99**, 697-707, doi:10.1016/j.bpj.2010.04.073 (2010).